C. R. Mecanique 344 (2016) 78–94

Contents lists available at ScienceDirect

Comptes Rendus Mecanique

www.sciencedirect.com

XFEM simulation of a quenched cracked glass plate with moving convective boundaries

Diyako Ghaffari, Samrand Rash Ahmadi *, Farzin Shabani

Faculty of Engineering, Mechanical Engineering Department, Urmia University, Urmia, Iran

ARTICLE INFO

Article history:
Received 3 May 2015
Accepted 28 September 2015
Available online 2 December 2015

Keywords:
XFEM
Quenched cracked glass plate
Moving convective boundaries
Transient heat conduction
Crank–Nicolson method

ABSTRACT

A moving quenched soda-lime glass plate with an initial edge crack is modeled, applying the eXtended finite-element method (XFEM) in order to investigate the stress field components and Von Mises stress around the crack. The convective heat with moving boundaries is considered in thermal formulation. The Crank–Nicolson time integration scheme is reformed and adjusted with a view to accurately solving the system of transient heat conduction matrix equations. In order to simulate the whole stages of the problem formulation, MATLAB XFEM (MXFEM) codes are written and employed. The stress distribution contours are plotted in detail and the stress fields around the crack tip are compared quantitatively. The variations of stress intensity factors (SIFs) during crack propagation are obtained through the calculation of the domain form of the interaction integral. In order to verify the procedure and display the ability of the developed formulation, the results are compared with experimental outputs from the literature.

1. Introduction

Modeling crack propagation in a standard finite-element framework is laborious due to the need for the mesh to match the geometry of the discontinuity. This becomes a serious difficulty when treating problems with evolving discontinuities, where the mesh must be reproduced at each step. Furthermore, the crack tip singularity should be accurately represented through the approximation [1]. In reaction to this shortcoming, the traditional finite-element man evolved towards an extended one (XFEM), initially proposed by Belytschko and Black [2], i.e. a powerful and accurate approach for solving discontinuity problems while utilizing the notion of partition of unity, based on a standard Galerkin procedure accommodating the internal boundaries in the discrete model [3,4]. Some of the chief advantages of the XFEM, which reproduce the singular field near a crack tip avoiding cumbersome remeshing procedures, are its remarkable flexibility for crack growth problems, and the simple formulation and independent definition of the crack from the FEM mesh it involves [5]. Of course, this method needs a variable number of degrees of freedom per node, which can be considered its only drawback [6]. In the area of fracture mechanics, the XFEM has been the subject of considerable researches in the last decade [7], one of which is thermoelastic fracture mechanics through XFEM that was investigated in detail by Duflot [8], who considered both 2D and 3D problems with different crack face thermal boundary conditions.

The study of thermoelastic fracture mechanics, which deals with the events of calamitous spreading of present cracks exposed to thermal loading, is considered to be essential in the design of many structures [9]. Structures such as glass

* Corresponding author.
E-mail address: s.rashahmadi@urmia.ac.ir (S. Rash Ahmadi).

http://dx.doi.org/10.1016/j.crme.2015.09.007
1631-0721/

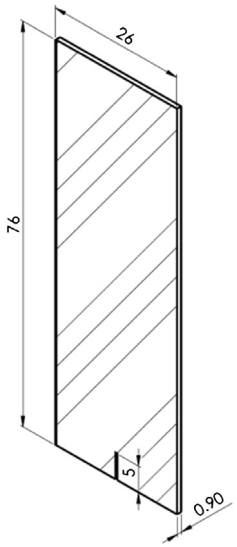

Fig. 1. Geometry of the specimen.

products can suffer sudden failure and catastrophic fracture, particularly in the presence of pre-existing cracks. Therefore, it is important to investigate the crack-growth behavior in glasses under thermal loading [10]. For the same reason, different analytical, experimental, and numerical studies have been reported to explain the mechanics of glass cracking [11–20]. All patterns of cracks, including straight, branched, and oscillating ones in thin glass plates subjected to thermal loads have been reported by Yuse and Sano [21]. Temperature jump and rapid cooling can affect the regulation of these patterns. Moreover, crack growth velocity can be controlled easily, and the cracks can be observed directly [22,23]. Yoneyama and co-workers experimentally assessed stress fields around a propagating crack tip in a quenched glass plate through instantaneous phase-stepping photoelasticity [24,25]. Afterwards, the variation of the crack tip stress fields during crack propagation has been studied [26–28]. Later, for the same problem, they also applied an experimental–numerical hybrid method to analyze the stress field at the crack tip [29], as well as they evidenced that the compressive stress fields are distributed around the tensile stresses at the crack tip, which leads to both a higher stress intensity factor and crack oscillation.

As can be observed from the viewpoint of thermoelastic fracture mechanics, the study and the understanding of the mechanics of complicated crack growth in glasses is an attractive and also necessary subject for designing structural components and machines. However, despite the great amount of works that have been done in these fields, there is no comprehensive satisfactory work that appropriately explains this phenomenon by considering the main parameters affected.

In this study, the eXtended Finite Element Method is implemented to model the effect of the transient heat conduction in a moving quenched thin soda-lime glass plate with an initial edge crack. The simultaneous effects of the movement of boundaries and of convection heat transfer in boundaries are taken into account in the thermal formulation. For obtaining the accurate temperatures from the system of ODE matrix equations, the Crank–Nicolson method is reformed and adjusted. The stress fields are analyzed around the crack, and the stress counters are plotted. The results illustrate that a compressive stress region is distributed around the tensile stress area at the crack tip, as it was reported in [29]. In addition, to study the crack propagation behavior, stress intensity factors are obtained versus time, using the calculation domain form of the interaction integral.

2. Problem statement

A thin soda-lime glass plate is considered, as shown in Fig. 1. The dimensions of the specimen are 26 mm in width, 76 mm in height, and 0.9 mm in thickness. It has a 5-mm-long initial edge crack in its bottom, which is supposed to have been created by a local temperature gradient using a soldering iron after scratching the sample by a glass cutter. Then, in order to apply a thermal load to the specimen, it is heated in a furnace up to a constant temperature T_h. Next, the specimen, as illustrated in Fig. 2, is translated vertically by a motor from a furnace to a cold bath. The distance from the top of the cold bath to the bottom of the furnace is 30 mm. The specimen enters the cold bath at a constant speed V. The cold bath is filled with water at a temperature $T_{\mathbf{c}}$, and the crack starts to propagate. More details about the experimental procedure are given in [25–29].

In this paper, we suppose that the plate is isotropic and homogeneous, and that all thermophysical properties like thermal conductivity, heat capacity, and density are temperature independent, and, since the plate is very thin, all operations are calculated assuming plane stress conditions.

Two aspects of the confronted issue that have to be considered are thermal and elastic parts. The thermal part is a transient heat-conducting problem with moving boundaries. Indeed, in every specified time, a time-dependent heat conduction

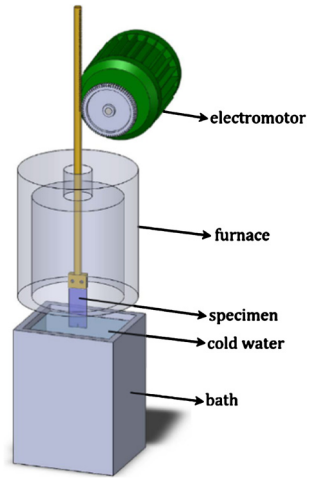

Fig. 2. Schematic design of the experiment.

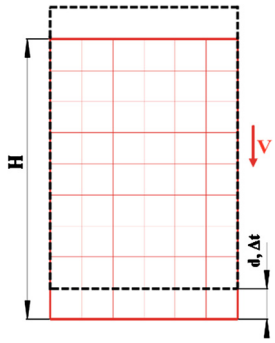

Fig. 3. A partial displacement of the plate into the cold bath in one time step.

problem with a new boundary and initial conditions has appeared, and their conditions depend on the prior moment. Therefore, it is important to solve the problem accurately in every step, because its result impacts the outputs of the next step as well as the mechanical part of the problem. Because of the low thermal conductivity and relatively high heat capacity of the material, the dominant factor that caused the cooling of the specimen in the cold bath is the convective boundary condition. Thus, for increasing the accuracy of the model, it is assumed that both surfaces and edges of the plate make convective thermal exchanges in the cold bath as well as in the outdoors of the specimen. Nevertheless, since the length between the furnace and the bath is less than the length of the specimen, when the specimen enters the cold bath, its other side is still located in the furnace, and its temperature is regarded to be the same as the furnace temperature; consequently, there is no convective heat transfer in this part.

For the elastic part, an indirect and implicit approach has been employed. Instead of computing the new mechanical formulation resulting from the thermal loads, like stress fields, interaction integral and stress intensity factors, the equivalent mechanical force arising from the generated thermal strain due to temperature variations is obtained. After calculation of the displacement field, the other requirements for the analysis of the problem can be computed.

The finite-element mesh of the plate is considered in such a way that the distance travelled by the plate per time step is equal to the length of the mesh elements. On the other hand, the incremental advancement of the plate into the cold bath in each step is associated with the entrance of elements located in a single row into the cold bath (Fig. 3). So, the time steps and the total time for complete entrance of the plate can be calculated simply as:

$$\Delta t = \frac{d}{V}$$

$$\text{total time} = \frac{H}{V}$$

where d is the length of the mesh elements in both directions, V is the constant vertical velocity of the plate, and H is its height. As it has been reported in several experimental works [25–28], the velocity of straight crack propagation is almost the same as that of the moving plate. So, for modeling this, the magnitude of the incremental crack growth in each step has been assumed to be equal to the length of the mesh elements.

3. XFEM problem formulation

3.1. XFEM discretization

The extended finite-element method along with the level set method allows discontinuities to be represented independently of the finite element mesh by using the partition of the unity finite-element method [30,31]. This method enriches all elements cut by a discontinuity with additional nodal degrees of freedom and by using enrichment functions satisfying the discontinuous behavior [2,32]. In general, the XFEM displacement approximation can be expressed as:

$$u(X) = u_{\mathrm{STD}}(X) + u_{\mathrm{ENR}}(X)$$
$$u(X) = \sum_{i\in\Omega} N_i(X)\left(u_i + \sum_{i\in\Omega_d} E(X)e_i\right) \tag{1}$$

where Ω is the overall domain, Ω_d is the domain that encompasses discontinuities, $N_i(X)$ are the standard finite-element shape functions, $E(X)$ is the enrichment function utilized for the discontinuous domain, and u_i, e_i are the standard and enriched degrees of freedom (DOF), respectively. Notice that when $\Omega \cap \Omega_d = \emptyset$, the enrichment function $E(X)$ disappears. Since the discontinuities are not defined by the finite-element mesh, the level set method [33,34] is exploited to track the discontinuities [35].

The approximation in Eq. (1) does not satisfy the interpolation property; i.e., $u_i \neq u(X_i)$ owing to enriched degrees of freedom. A normal way to satisfy the interpolation property in applying XFEM is to shift the enrichment functions [36] as:

$$S_i(X) = E(X) - E_i(X)$$

where $S_i(X)$ is the shifted enrichment function for the ith node and $E_i(X)$ is the value of $E(X)$ at the ith node. For modeling a crack in a homogeneous material, for an element completely cut by a crack, the Heaviside [32] enrichment function is used as:

$$h(X) = \begin{cases} +1 & \text{above the crack} \\ -1 & \text{below the crack} \end{cases} \tag{2}$$

and so the shifted Heaviside enrichment function is:

$$H(X) = h(X) - h_i(X) \tag{3}$$

For an element containing the crack tip, the branch enrichment functions (asymptotic functions) [2,37] take the following form:

$$\{f_j(X)\}_{j=1}^{4} = \left\{\sqrt{r}\sin\frac{\theta}{2}, \sqrt{r}\cos\frac{\theta}{2}, \sqrt{r}\sin\theta\sin\frac{\theta}{2}, \sqrt{r}\sin\theta\cos\frac{\theta}{2}\right\} \tag{4}$$

and for the shifted branch, the enrichment functions are:

$$F(X) = f(X) - f_i(X) \tag{5}$$

In Eq. (4), r and θ are the polar coordinates in the local crack tip coordinate system and the first function represents the discontinuity near the tip, while the other three functions are added to get accurate results with relatively coarse meshes. Note that when a node should be enriched by both Eqs. (2) and (4), only Eq. (4) is used. Fig. 4 shows how the elements containing discontinuities are selected in two successive increments. The sandy brown elements and their squared nodes are those cut by the crack tip and enriched by the branch functions, while the light green elements and their circled nodes are those cut by the crack face and enriched by the Heaviside function, whereas the yellow elements are those enriched at their nodes by both enrichments.

Ultimately, the XFEM approximation of the displacement field is:

$$u(X) = \sum_{i} N_i(X)\left(u_i + H_i(X)a_i + \sum_{j=1}^{4} F_j(X)b_{ij}\right) \tag{6}$$

The two-dimensional form can be written as:

$$u(x,y) = \sum_{i\in n} N_i(x,y)u_i + \sum_{i\in n_h} N_i(x,y)H_i(x,y)a_i + \sum_{i\in n_c}\sum_{j=1}^{4} N_i(x,y)F_j(r,\theta)b_{ij} \tag{7}$$

where u_i are traditional degrees of freedom, a_i are additional degrees of freedom corresponding to the Heaviside enrichments, b_{ij} are additional degrees of freedom related to the crack-tip enrichments, n_h is a set of Heaviside enrichment nodes, and n_c is a set of crack-tip enrichment nodes.

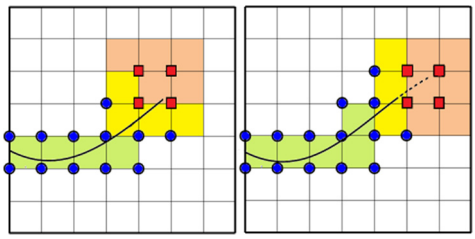

Fig. 4. The schematic of enrichment procedure; brown elements and their squared nodes are those cut by the crack tip and enriched by the branch functions, the green elements and their circled nodes are those cut by the crack face and enriched by the Heaviside function, and the yellow elements are those enriched at their nodes by both enrichments.

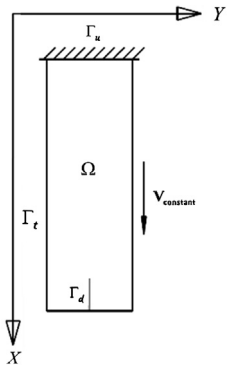

Fig. 5. The body with an internal crack that moves at a constant velocity.

In problems dealing with thermal fracture, the XFEM for temperature discontinuities can also be applicable. With the adiabatic crack assumption, the Heaviside function is suitable for elements cut by crack and having temperature jump. Concerning near-tip enrichment, the leading term of the asymptotic field for the temperature [8] can be written as:

$$T = -\frac{K_T}{k}\sqrt{\frac{2r}{\pi}}\sin\frac{\theta}{2}$$

where k is the thermal conductivity, K_T provides the strength of flux singularity at the crack tip. Therefore, the temperature field can be discretized like the displacement field, but with only the first branch function of Eq. (4), i.e.:

$$T(x,y,t) = \sum_{i\in n} N_i(x,y)T_i + \sum_{i\in n_h} N_i(x,y)H_i(x,y)A_i + \sum_{i\in n_c} N_i(x,y)F_1(r,\theta)B_i \tag{8}$$

where T_i, A_i, and B_i are unenriched, face-enriched, and tip-enriched unknown temperatures, respectively, and

$$F_1(r,\theta) = \sqrt{r}\sin\frac{\theta}{2} - \sqrt{r_i}\sin\frac{\theta_i}{2}$$

3.2. The elastic model

The problem is defined in the domain Ω bounded by Γ, as illustrated in Fig. 5, where $\Gamma = \Gamma_u \cup \Gamma_t$ and $\Gamma_u \cap \Gamma_t = \emptyset$. Newton's second law of motion and Hook's law for an isotropic homogeneous material are [38]:

$$\sigma_{ij,j} + b_j = \rho u_{j,tt} \quad i,j = 1,2,3 \tag{9}$$

$$\sigma_{ij} = \frac{E}{1+\nu}\left\{\varepsilon_{ij} + \frac{\nu}{1-2\nu}\varepsilon_{kk}\delta_{ij}\right\} - \frac{E\alpha\Delta T}{1-2\nu}\delta_{ij} \quad i,j = 1,2,3 \tag{10}$$

respectively, where σ_{ij} are Cauchy stress tensor components, b_j are body force vector components, u_j are displacement vector components, ε_{ij} are strain tensor components, ρ is the density, E is Young's modulus, ν is Poisson's ratio, α is the thermal expansion, and ΔT is the nodal temperature change.

Eq. (9) in two dimensions with constant velocity V (static equilibrium), in the absence of body forces, and Eq. (10) in plane stress conditions are reduced to:

$$\sigma_{ij,j} = 0 \quad i, j = 1, 2 \tag{11}$$

$$\sigma_{ij} = \frac{E}{1+\nu}\left\{\varepsilon_{ij} + \frac{\nu}{1-\nu}\varepsilon_{kk}\delta_{ij}\right\} - \frac{E\alpha\Delta T}{1-\nu}\delta_{ij} \quad i, j = 1, 2 \tag{12}$$

The boundary conditions are:

$$\begin{aligned} &\sigma_{ij}n_j = 0 \quad \text{on } \Gamma_t \\ &u = 0 \quad\quad\ \text{on } \Gamma_u \\ &\sigma_{ij}n_j = 0 \quad \text{on } \Gamma_d^+ \\ &\sigma_{ij}n_j = 0 \quad \text{on } \Gamma_d^+ \end{aligned} \tag{13}$$

Eq. (7) is substituted in the weak form of the combined Eqs. (11) and (12), applying the boundary conditions, and using the Bubnov–Galerkin method, a system of discrete linear equations is derived. The system of linear equations can be written in the form that is commonly associated with the finite-element method:

$$[K]\{U\} = \{F\} \tag{14}$$

where $\{U\} = \{u_i^u, u_i^v, a_i^u, a_i^v, b_{ij}^u, b_{ij}^v\}^{\mathrm{T}}$ is the vector of unknown displacement at the nodes, the superscripts u and v referring to x and y components of the displacement, respectively.

$[K]$ is the global stiffness matrix given by [39]:

$$[K] = \int_{\Omega} [B]^{\mathrm{T}}[C][B]\,\mathrm{d}\Omega \tag{15}$$

and $\{F\}$ is the equivalent thermal-load vector associated with the temperature variation over an element [40]:

$$\{F\} = \int_{\Omega} [B]^{\mathrm{T}}[C]\left\{\varepsilon^{\mathrm{th}}\right\}\mathrm{d}\Omega \tag{16}$$

where $\{\varepsilon^{\mathrm{th}}\}$ is the thermal strain vector that is defined for an isotropic material in plane stress conditions as:

$$\left\{\varepsilon^{\mathrm{th}}\right\} = \begin{Bmatrix} \varepsilon_{xx}^{\mathrm{th}} \\ \varepsilon_{yy}^{\mathrm{th}} \\ \varepsilon_{xy}^{\mathrm{th}} \end{Bmatrix} = \begin{Bmatrix} 1 \\ 1 \\ 0 \end{Bmatrix} \alpha\Delta T \tag{17}$$

in which $\Delta T = T_t - T_{t-\Delta t}$ is obtained in Section 3.3.1 and the other terms of $[K]$ and $\{F\}$ are defined in the Appendix.

The vector of $\{F\}$ and the matrix of $[K]$, in terms of their elements, are as follows:

$$\{F\} = \left\{\left\{F_u^u\right\} \quad \left\{F_u^v\right\} \quad \left\{F_a^u\right\} \quad \left\{F_a^v\right\} \quad \left\{F_b^u\right\} \quad \left\{F_b^v\right\}\right\}^{\mathrm{T}} \tag{18}$$

$$[K] = \begin{bmatrix} [K_{uu}^{uu}] & [K_{uu}^{uv}] & [K_{ua}^{uu}] & [K_{ua}^{uv}] & [K_{ub}^{uu}] & [K_{ub}^{uv}] \\ & [K_{uu}^{vv}] & [K_{ua}^{vu}] & [K_{ua}^{vv}] & [K_{ub}^{vu}] & [K_{ub}^{vv}] \\ & & [K_{aa}^{uu}] & [K_{aa}^{uv}] & [K_{ab}^{uu}] & [K_{ab}^{uv}] \\ & & & [K_{aa}^{vv}] & [K_{ab}^{vu}] & [K_{ab}^{vv}] \\ & \text{Sym.} & & & [K_{bb}^{uu}] & [K_{bb}^{uv}] \\ & & & & & [K_{bb}^{vv}] \end{bmatrix} \tag{19}$$

where $[K_{uu}]$ is the stiffness matrix of the traditional finite-element method for the unenriched DOF that encompasses the large portion of the global stiffness matrix and will be constant at each step of crack growth, $[K_{ua}]$ and $[K_{ub}]$ are coupled matrices of enriched and traditional DOF, $[K_{aa}]$ and $[K_{bb}]$ are the stiffness matrices corresponding to enriched DOF. The same explanation can be given for the $\{F\}$ vector.

Let us mention that the displacement of the nodes satisfied by the second boundary conditions is zero. Hence, the nodal displacement should be computed for the other free nodes as following:

$$\{U_r\} = [K_{rr}]^{-1}\{F_r\} \tag{20}$$

where $\{U_r\}$ are the free nodes rows in the displacement vector, $[K_{rr}]$ are the free nodes rows and columns in the stiffness matrix, and $\{F_r\}$ are the free nodes rows of the force vector. After computing the nodal displacement vector, the components of strain and stress fields as well as Von Mises stress (see Appendix) around the crack and in the whole plate can be attained without difficulty. SIFs for the plane stress conditions can be obtained by using the domain form of the interaction integral, as follows [31]:

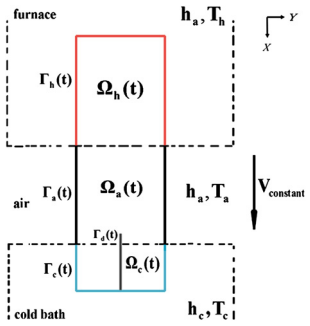

Fig. 6. Schematic design of the problem domain.

$$K_{\mathrm{I}}^{(1)} = \frac{E}{2} M^{(1,\text{state one})} \tag{21}$$

$$K_{\mathrm{II}}^{(1)} = \frac{E}{2} M^{(1,\text{state two})} \tag{22}$$

where

$$M^{(1,2)} = \int_A \left[\sigma_{ij}^{(1)} \frac{\partial u_i^{(2)}}{\partial x_1} + \sigma_{ij}^{(2)} \frac{\partial u_i^{(1)}}{\partial x_1} - W^{(1,2)} \delta_{1j} \right] \frac{\partial q}{\partial x_j} \, \mathrm{d}A \tag{23}$$

with

$$W^{(1,2)} = \sigma_{ij}^{(1)} \varepsilon_{ij}^{(2)} = \sigma_{ij}^{(2)} \varepsilon_{ij}^{(1)}$$

$$q = \sum_{i=1}^{4} N_i q_i$$

K_{I} is the mode-I stress intensity factor, K_{II} is the mode-II stress intensity factor, $M^{(1,2)}$ is the domain form of the interaction integral. Superscript 1 denotes the actual state corresponding to the stress and displacement fields of the XFEM analysis, superscript 2 denotes the auxiliary state that has been chosen by Westergaard [41] and by Williams [42] for stress and displacement equations. The term of 'state one' is the auxiliary state as pure mode I, 'state two' is the auxiliary state as pure mode II. E is Young's modulus, $W^{(1,2)}$ is the interaction/mutual strain energy of the body, q is defined as an arbitrary smooth function; standard finite-element shape functions have been used to interpolate its value.

A free MATLAB XFEM code [43] was reformed and has been applied for the presentation of elastic problem formulation. For FEM integrals on unenriched elements, a standard Gauss quadrature rule is used; however, for elements containing discontinuities, due to the high gradient and the existence of singularity, the technique based on subdividing quadrangles into triangles and integrating over each triangle is applied to avoid difficulties with integrating the discontinuous domain and to enhance the accuracy of the numerical integration.

3.3. The thermal model

Recall that the problem is in the domain Ω bounded by Γ and is moving downward with constant velocity V, as illustrated in Fig. 6. In this figure:

- $\Omega_h(t)$ is the hot region in the furnace bounded by $\Gamma_h(t)$ and the domain decreases over time,
- $\Omega_c(t)$ is the cold region in the water bath bounded by $\Gamma_c(t)$ and the domain increases over time,
- $\Omega_a(t)$ is the remaining region that is assumed to be subjected to air at room temperature (standard temperature), bounded by $\Gamma_a(t)$, the domain decreasing over time,
- $\Gamma_d(t)$ is the crack boundary that is considered to be adiabatic and to consist of two coincident boundaries $\Gamma_d(t)^+$ and $\Gamma_d(t)^-$.

So it can be readily written that:

$$\Omega_h(t) \cup \Omega_c(t) \cup \Omega_a(t) = \Omega \quad \text{and} \quad \Omega_h(t) \cap \Omega_c(t) \cap \Omega_a(t) = \emptyset$$

$$\Gamma_h(t) \cup \Gamma_c(t) \cup \Gamma_a(t) = \Gamma \quad \text{and} \quad \Gamma_h(t) \cap \Gamma_c(t) \cap \Gamma_a(t) = \emptyset$$

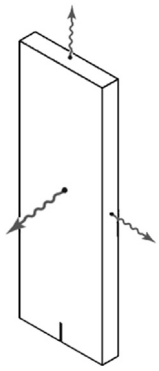

Fig. 7. The plate's edge and surface convection that is considered in the formulation.

with the assumption of temperature independence for the thermophysical properties, the general heat conduction equation for the moving solid, which is derived from the first law of thermodynamics, and the Fourier law equation are expressed as [44]:

$$\frac{\partial q_i}{\partial x_i} + \rho c_p \frac{DT}{Dt} = Q \quad i = 1, 2, 3 \tag{24}$$

$$q_i = -k_i \frac{\partial T}{\partial x_i} \quad i = 1, 2, 3 \tag{25}$$

respectively. Where $\frac{D}{Dt}$ is the substantial derivative, the q_is are the heat flux vector components, c_p is the isobaric mass heat capacity, Q is the thermal heat generation rate, and k_is are the components of the thermal conductivity vector.

For an isotropic thin plate, with a heat convective surface [45] and without a thermal source that moves vertically at a constant velocity, the above two-dimensional equations are:

$$\frac{\partial q_i}{\partial x_i} + \rho c_p \left(\frac{\partial T}{\partial t} + u_{x_1} \frac{\partial T}{\partial x_1} \right) + 2h(T - T_\infty) = 0 \quad i = 1, 2 \tag{26}$$

$$q_i = -k \frac{\partial T}{\partial x_i} \quad i = 1, 2 \tag{27}$$

where h is the convection coefficient, and T_∞ is the ambient temperature of the surrounding fluid. It is mentioned that, since the surfaces of the thin plate are not assumed to be adiabatic, the third term on the left-hand side of Eq. (26) appears to be due to the first law of thermodynamics.

The initial conditions of the problem are given by:

$$\begin{aligned} &T(x, y, 0) = T_h \quad \text{in } \Omega \\ &T_i\left(x, y, t + \frac{\Delta t}{n}\right) = T(x, y, t) \quad \text{in } \Omega \end{aligned} \tag{28}$$

where T_i is the initial temperature and the boundary conditions are:

$$\begin{aligned} &\forall (P, t) \in \Omega_h(t) \rightarrow T(P, t) = T_h \\ &\forall (P, t) \in \Gamma_h(t) \rightarrow q_i n_i = 0 \\ &\forall (P, t) \in \left(\Gamma_d^+(t) \cup \Gamma_d^-(t)\right) \rightarrow q_i n_i = 0 \\ &\forall (P, t) \in \Gamma_c(t) \rightarrow q_i n_i = h_c\left(T(P, t) - T_c\right) \\ &\forall (P, t) \in \Gamma_a(t) \rightarrow q_i n_i = h_a\left(T(P, t) - T_a\right) \end{aligned} \tag{29}$$

where T_h, T_c, T_a are the temperatures of furnace, cold water, air, and h_c, h_a are the convection coefficients of cold water and air, respectively. The surface convection and the edge convection of the plate are shown in Fig. 7.

Notice that the initial conditions will be explained and implemented in Section 3.3.1.

By substituting Eq. (27) into Eq. (26):

$$k \frac{\partial^2 T}{\partial x^2} + k \frac{\partial^2 T}{\partial y^2} - \rho c_p V \frac{\partial T}{\partial x} + 2h(T - T_\infty) = \rho c_p \frac{\partial T}{\partial t} \tag{30}$$

after substituting the XFEM discretized temperature field, Eq. (8), into Eq. (30), using the Galerkin finite-element method, as well as Green's theorem in the plane and finally applying the boundary conditions of the problem, except the first one, the global system of linear ODE equations can be written as:

$$\left[C^{\mathrm{th}}\right]\{\dot{T}\}+\left[K^{\mathrm{th}}\right]\{T\}=\left\{F^{\mathrm{th}}\right\} \tag{31}$$

where $\{T\}=\{T_i, A_i, B_i\}^{\mathrm{T}}$ is the vector of unknown temperatures at the nodes. Notice that if the thermophysical properties are temperature dependent, the above equations are nonlinear.

$[C^{\mathrm{th}}]$ is the global capacitance matrix defined by:

$$\left[C^{\mathrm{th}}\right]=\int_{\Omega}\rho c_p[\Psi]^{\mathrm{T}}[\Psi]\,\mathrm{d}\Omega \tag{32}$$

and $[K^{\mathrm{th}}]$ is the global conductance matrix that can be shown as:

$$\left[K^{\mathrm{th}}\right]=[K_D]+[K_V]+[K_{hs}]+[K_{he}] \tag{33}$$

where

$$[K_D]=\int_{\Omega}\left[B^{\mathrm{th}}\right]^{\mathrm{T}}[D]\left[B^{\mathrm{th}}\right]\mathrm{d}\Omega \tag{34}$$

$$[K_V]=\int_{\Omega}[\Phi]\left[V^{\mathrm{th}}\right]\left[B^{\mathrm{th}}\right]\mathrm{d}\Omega \tag{35}$$

$$[K_{hs}]=\int_{\Omega}2h[\Psi]^{\mathrm{T}}[\Psi]\,\mathrm{d}\Omega=\iint_{A_c(t)}2h_c[\Psi]^{\mathrm{T}}[\Psi]\,\mathrm{d}A_c+\iint_{A_a(t)}2h_a[\Psi]^{\mathrm{T}}[\Psi]\,\mathrm{d}A_a \tag{36}$$

$$[K_{he}]=\int_{\Gamma}h[\Psi]^{\mathrm{T}}[\Psi]\,\mathrm{d}\Gamma=\oint_{S_c(t)}h_c[\Psi]^{\mathrm{T}}[\Psi]t\,\mathrm{d}S_c+\oint_{S_a(t)}h_a[\Psi]^{\mathrm{T}}[\Psi]t\,\mathrm{d}S_a \tag{37}$$

with

$$\Phi=\begin{bmatrix}\Psi^{\mathrm{T}} & \Psi^{\mathrm{T}}\end{bmatrix} \tag{38}$$

$$V^{\mathrm{th}}=\begin{bmatrix}\rho c_p V & 0\\ 0 & 0\end{bmatrix} \tag{39}$$

where t, A and S are the thickness, the surface and the periphery of the plate, whereas the other terms of global capacitance and conductance matrices are defined in the Appendix. Note that Eq. (35) arises from the movement of the plate, and that Eq. (36) results from the surface convection of the plate, while Eq. (37) corresponds to the edge convection of the plate.

$\{F^{\mathrm{th}}\}$ is the thermal force vector that is expressed as:

$$\left\{F^{\mathrm{th}}\right\}=\{f_{hs}\}+\{f_{he}\} \tag{40}$$

where

$$\{f_{hs}\}=\int_{\Omega}2hT_{\infty}[\Psi]^{\mathrm{T}}\,\mathrm{d}\Omega=\iint_{A_c(t)}2h_cT_c[\Psi]^{\mathrm{T}}\,\mathrm{d}A_c+\iint_{A_a(t)}2h_aT_a[\Psi]^{\mathrm{T}}\,\mathrm{d}A_a \tag{41}$$

$$\{f_{he}\}=\int_{\Gamma}hT_{\infty}[\Psi]^{\mathrm{T}}\,\mathrm{d}\Gamma=\oint_{S_c(t)}h_cT_c[\Psi]^{\mathrm{T}}t\,\mathrm{d}S_c+\oint_{S_a(t)}h_aT_a[\Psi]^{\mathrm{T}}t\,\mathrm{d}S_a \tag{42}$$

again Eq. (41) and Eq. (42) result from surface convection and edge convection, respectively.

The matrices of $[C^{\mathrm{th}}]$ and $[K^{\mathrm{th}}]$ and the vectors of $\{F^{\mathrm{th}}\}$ in terms of their elements are:

$$\left[C^{\mathrm{th}}\right]=\begin{bmatrix}[C^{\mathrm{th}}_{TT}] & [C^{\mathrm{th}}_{TA}] & [C^{\mathrm{th}}_{TB}]\\ [C^{\mathrm{th}}_{AT}] & [C^{\mathrm{th}}_{AA}] & [C^{\mathrm{th}}_{AB}]\\ [C^{\mathrm{th}}_{BT}] & [C^{\mathrm{th}}_{BA}] & [C^{\mathrm{th}}_{BB}]\end{bmatrix} \tag{43}$$

$$\left[K^{\mathrm{th}}\right]=\begin{bmatrix}[K^{\mathrm{th}}_{TT}] & [K^{\mathrm{th}}_{TA}] & [K^{\mathrm{th}}_{TB}]\\ [K^{\mathrm{th}}_{AT}] & [K^{\mathrm{th}}_{AA}] & [K^{\mathrm{th}}_{AB}]\\ [K^{\mathrm{th}}_{BT}] & [K^{\mathrm{th}}_{BA}] & [K^{\mathrm{th}}_{BB}]\end{bmatrix} \tag{44}$$

Explanations similar to those of Eq. (19) can be invoked for the subscripts of the above matrices and the thermal force vector.

3.3.1. The adjusted Crank–Nicolson method

At first, it should be mentioned that in addition to temperature, which is varied versus time, the conductance matrix and the thermal force vector are also changed with time. As it was shown formerly, both of them have a time-variable domain/boundary integration, in which the h and T_∞ terms are continuously changing for the nodes that are crossing from the borders of the furnace, bath, and outdoors. Apart from these, for both matrices, capacitance, conductance and thermal force vector, at each step, new elements emerge due to crack growth and the additional degrees of freedom for enriching new increments of the crack. These elements are assumed to be zero for the prior time steps of the matrices and the vector.

Another point is that the first thermal boundary condition of the problem is still not applied. It was:

$$\forall (P,t) \in \Omega_h(t) \rightarrow T(P,t) = T_h \tag{45}$$

For applying this boundary condition, the global system of ODE equations in Eq. (31) is partitioned as:

$$\begin{bmatrix} C_{ss}^{\text{th}} & C_{su}^{\text{th}} \\ C_{us}^{\text{th}} & C_{uu}^{\text{th}} \end{bmatrix} \begin{Bmatrix} \dot{T}_s \\ \dot{T}_u \end{Bmatrix} + \begin{bmatrix} K_{ss}^{\text{th}} & K_{su}^{\text{th}} \\ K_{us}^{\text{th}} & K_{uu}^{\text{th}} \end{bmatrix} \begin{Bmatrix} T_s \\ T_u \end{Bmatrix} = \begin{Bmatrix} F_s^{\text{th}} \\ F_u^{\text{th}} \end{Bmatrix} \tag{46}$$

where the subscript u denotes terms associated with unknown (active) temperatures and the subscript s denotes terms associated with specified (constrained) temperatures. It is obvious that:

$$T_s = T_h$$
$$\dot{T}_s = 0$$

So for the unknown temperatures, the partitioned equations can be written as:

$$\left[C_{uu}^{\text{th}}\right]\{\dot{T}_u\} + \left[K_{uu}^{\text{th}}\right]\{T_u\} = \left\{F_u^{\text{th}}\right\} - \left[K_{us}^{\text{th}}\right]\{T_h\} \tag{47}$$

which now appropriately takes into account the effects of specified temperatures as forcing functions on the right-hand side.

For obtaining the transient temperatures in each step, the generalized trapezoidal approximation [46] is adopted for numerically integrating the systems of ODE equations in Eq. (31). According to this technique, the temperatures at the time level $p+1$ are:

$$\{T\}^{p+1} = \{T\}^p + \left[(1-\theta)\{\dot{T}\}^p + \theta\{\dot{T}\}^{p+1}\right]\frac{\Delta t}{n} \tag{48}$$

where Δt, as previously defined, is the time for elements in a row to enter the bath in each step, $\frac{\Delta t}{n}$ is the time substep between time levels p and $p+1$, and θ is the temporal parameter that takes values between 0 and 1. The above equation for the unknown temperatures can be written as:

$$\{T_u\}^{p+1} = \{T_u\}^p + \left[(1-\theta)\{\dot{T}_u\}^p + \theta\{\dot{T}_u\}^{p+1}\right]\frac{\Delta t}{n} \tag{49}$$

For time levels denoted as p and $p+1$, the global system of ODE – (34) – can be written as follows:

$$\left[C^{\text{th}}\right]^p\{\dot{T}\}^p + \left[K^{\text{th}}\right]^p\{T\}^p = \left\{F^{\text{th}}\right\}^p \tag{50}$$
$$\left[C^{\text{th}}\right]^{p+1}\{\dot{T}\}^{p+1} + \left[K^{\text{th}}\right]^{p+1}\{T\}^{p+1} = \left\{F^{\text{th}}\right\}^{p+1} \tag{51}$$

Eqs. (50) and (51) for the unknown temperatures, in the form of Eq. (47), are:

$$\left[C_{uu}^{\text{th}}\right]^p\{\dot{T}_u\}^p + \left[K_{uu}^{\text{th}}\right]^p\{T_u\}^p = \left\{F_u^{\text{th}}\right\}^p - \left(\left[K_{us}^{\text{th}}\right]\{T_h\}\right)^p \tag{52}$$
$$\left[C_{uu}^{\text{th}}\right]^{p+1}\{\dot{T}_u\}^{p+1} + \left[K_{uu}^{\text{th}}\right]^{p+1}\{T_u\}^{p+1} = \left\{F_u^{\text{th}}\right\}^{p+1} - \left(\left[K_{us}^{\text{th}}\right]\{T_h\}\right)^{p+1} \tag{53}$$

The above equations are substituted into Eq. (49), which, after some simplification, yields:

$$\left(\frac{n}{\Delta t}\left[C_{uu}^{\text{th}}\right]^{p+1} + \theta\left[K_{uu}^{\text{th}}\right]^{p+1}\right)\{T_u\}^{p+1}$$
$$= \left(\frac{n}{\Delta t}\left[C_{uu}^{\text{th}}\right]^p - (1-\theta)\left[K_{uu}^{\text{th}}\right]^p\right)\{T_u\}^p + \left(\theta\left(\left\{F_u^{\text{th}}\right\} - \left[K_{us}^{\text{th}}\right]\{T_h\}\right)^{p+1} + (1-\theta)\left(\left\{F_u^{\text{th}}\right\} - \left[K_{us}^{\text{th}}\right]\{T_h\}\right)^p\right) \tag{54}$$

for different values of θ, different transient schemes have appeared. For $\theta = \frac{1}{2}$, the semi-implicit scheme, the Crank–Nicolson method is obtained as following:

$$\left(\frac{n}{\Delta t}\left[C_{uu}^{\mathrm{th}}\right]^{p+1}+\frac{1}{2}\left[K_{uu}^{\mathrm{th}}\right]^{p+1}\right)\{T_u\}^{p+1}$$
$$=\left(\frac{n}{\Delta t}\left[C_{uu}^{\mathrm{th}}\right]^{p}-\frac{1}{2}\left[K_{uu}^{\mathrm{th}}\right]^{p}\right)\{T_u\}^{p}+\frac{1}{2}\left(\left(\left\{F_u^{\mathrm{th}}\right\}-\left[K_{us}^{\mathrm{th}}\right]\{T_h\}\right)^{p+1}+\left(\left\{F_u^{\mathrm{th}}\right\}-\left[K_{us}^{\mathrm{th}}\right]\{T_h\}\right)^{p}\right) \tag{55}$$

This method is unconditionally stable. However, the approximate solutions can exhibit spurious oscillations due to the unfit selection of the time substep, whereas these oscillations do not occur in reality [46,47]. To arrive at an appropriate time substep, Von Neumann's stability analysis can be employed [48]. For this problem, it can be written as:

$$\frac{\kappa\left(\frac{\Delta t}{n}\right)}{d^2}\leq\frac{1}{2} \tag{56}$$

where κ is the thermal diffusivity, and d, as defined formerly, is the length of mesh elements. Using the equality in the above equation, the minimum number of substeps for each step can be obtained as:

$$n=\frac{2\kappa\,\Delta t}{d^2} \tag{57}$$

Substituting Eq. (57) into Eq. (55), the transient temperatures at time level $p+1$ are:

$$\{T_u\}^{p+1}=[A]^{-1}\left([B]\{T_u\}^{p}+\frac{1}{2}\left(\{F\}^{p+1}+\{F\}^{p}\right)\right) \tag{58}$$

$$[A]=\frac{2\kappa}{d^2}\left[C_{uu}^{\mathrm{th}}\right]^{p+1}+\frac{1}{2}\left[K_{uu}^{\mathrm{th}}\right]^{p+1} \tag{59}$$

$$[B]=\frac{2\kappa}{d^2}\left[C_{uu}^{\mathrm{th}}\right]^{p}-\frac{1}{2}\left[K_{uu}^{\mathrm{th}}\right]^{p} \tag{60}$$

$$\{F\}=\left\{F_u^{\mathrm{th}}\right\}-\left[K_{us}^{\mathrm{th}}\right]\{T_h\} \tag{61}$$

It should be mentioned that the initial conditions are not still applied. They were:

$$T(x,y,0)=T_h \qquad \text{in } \Omega$$
$$T_i\left(x,y,t+\frac{\Delta t}{n}\right)=T(x,y,t) \qquad \text{in } \Omega$$

According to the initial conditions, Eq. (58) is supplemented as:

- for the first time levels, $p+1$ and p, at $t=0$:

$$\{T_u\}^{p+1}=[A]^{-1}\left([B]\{T_h\}+\frac{1}{2}\left(\{F\}^{p+1}+\{F\}^{p}\right)\right) \quad \text{where} \begin{cases} p\cong(t=0) \\ p+1\cong(t=\frac{\Delta t}{n}) \end{cases} \tag{62}$$

  which this is the first substep for obtaining the unknown temperatures of the next step, $\{T_u(\Delta t)\}$;
- for the first time levels, $p+1$ and p, at $t=t$ (any other time):

$$\{T_u\}^{p+1}=[A]^{-1}\left([B]\left\{T_u(t)\right\}+\frac{1}{2}\left(\{F\}^{p+1}+\{F\}^{p}\right)\right) \quad \text{where} \begin{cases} p\cong(t=t) \\ p+1\cong(t=t+\frac{\Delta t}{n}) \end{cases} \tag{63}$$

  where $\{T_u(t)\}$ is the ultimate temperature of the previous step and has been attained formerly, and Eq. (63) is the first substep for obtaining the unknown temperatures of the next step, $\{T_u(t+\Delta t)\}$.

Now with these considerations, the transient temperatures vector in each step can be achieved. And through subtracting the temperature vectors of a step from the previous one, the temperature variation can be obtained over an element. It is mentioned that the temperature fields are acquired by substituting the nodal unknown transient temperatures in Eq. (8). Finally, the elemental temperature variations are substituted in Eq. (17), after obtaining the thermal strain of an element, and substituting it in Eq. (16), the equivalent thermal loads associated with temperature variations are attained. After having obtained this, the displacement vector and other mechanical parameters can be reached.

The MATLAB codes have been written for the presentation of thermal XFEM problem formulations, and it has been merged with the elastic part, to completely simulate the problem with the extended finite-element method.

Table 1
The properties of the plate and of the surrounding fluids [29,44].

E	Young's modulus	71.6 GPa
ν	Poisson's ratio	0.20
ρ	Density of plate	2500 kg/m^3
k	Thermal conductivity	1.005 J/m s K
α	Thermal expansion coefficient	8.7 $\times$ (10^{-6}) 1/K
c_p	Isobaric mass heat capacity	921 J/kg K
κ	Thermal diffusivity	4.36 $\times$ (10^{-7}) m^2/s
h_w	Convection coefficient of the water	440 J/m^2 s K
h_a	Convection coefficient of the air	5 J/m^2 s K
T_w	Temperature of the cold water	290.2 K
T_a	Temperature of the air of outdoors	298 K
T_h	Temperature of the furnace	360 K
V	Velocity of the translated plate	0.0021 m/s

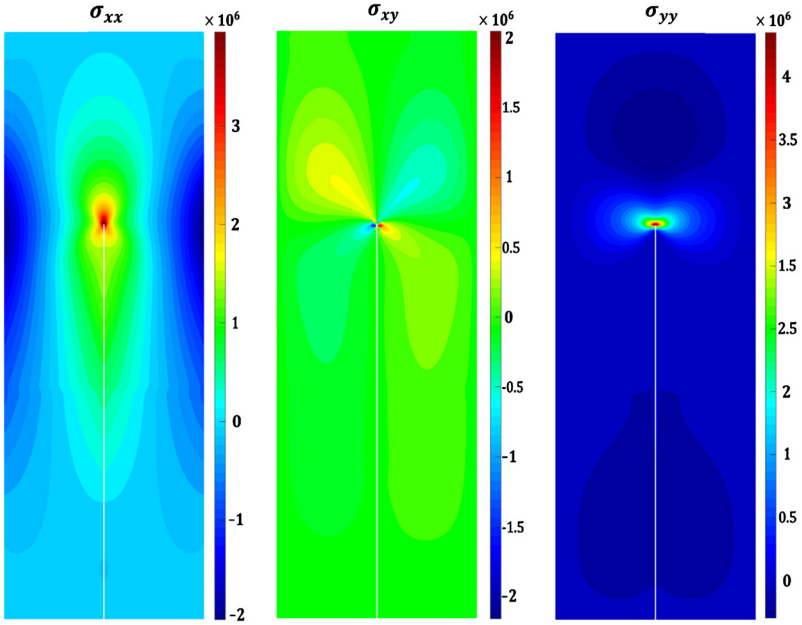

Fig. 8. Stress fields contours when the plate has completely exited the furnace.

4. Results and discussions

In order to illustrate the performance of the formulation framework, the numerical results are obtained for real mechanical and thermal properties. The properties of the material and of the surrounding fluids are presented in Table 1. The maximum hoop stress criterion is used for predicting the path of the crack propagation. As it was stated in Section 2, the distance travelled by the plate in each time step is equal to the length of the mesh elements, and in several experimental works [25–28] it has been reported that the straight crack growth velocity envisaged in this problem is almost the same as the velocity of the translated plate. Hence, for simulating this consideration, the magnitude of the crack growth increment in each time step is assumed equal to the length of mesh elements. Mesh resolutions for the numerical results is chosen such that the numbers of elements are 65×190, and the results are obtained for the time when the plate has completely exited the furnace. Notice that for these appointed time level, mesh resolution, and velocity of the plate (in Table 1), the number of time steps is $N_{\mathrm{TS}} = 115$. The contours of the stress field components as well as the Von Mises stress are shown in Fig. 8 and Fig. 9.

As it is observed, the stress field contours show that a compressive stress region is distributed around the tensile stress area at the crack tip, which can be considered as a main cause of a higher value of the K_{I}. This result as well as the contours of stress field distributions are in good agreement with the experimental results presented in [29]. By considering the higher value of the K_{I} and the negligible value of K_{II} (as it was reported in [26–28]), from the maximum hoop stress criterion, it can be expressed that the crack propagates with the K_{I} dominant condition and the crack growth path is straight as it was presented in [26–28] (Fig. 10). The values of SIFs during crack propagation are displayed in Fig. 11. As previously mentioned, because of the low thermal conductivity and relatively high specific heat of the glass, the dominant factor that caused the plate to cool is the boundaries of the plate that was located in the cold bath. So at the time the plate enters the bath, there

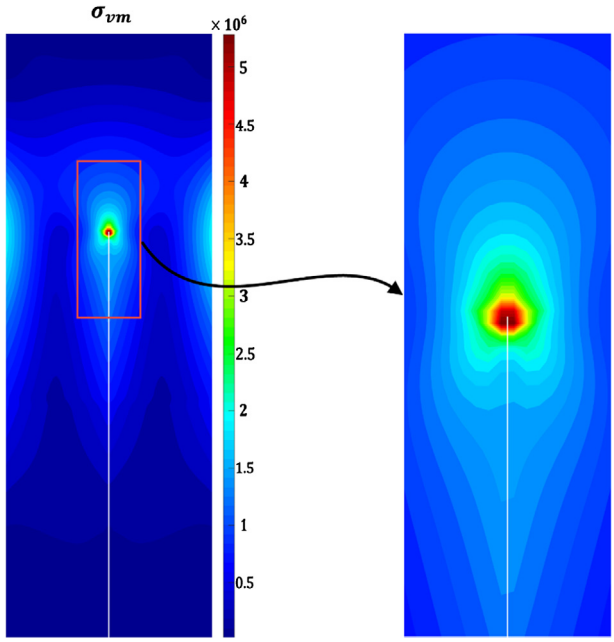

Fig. 9. (a) Von Mises' stress contour. (b) Magnification of the contour around the crack tip.

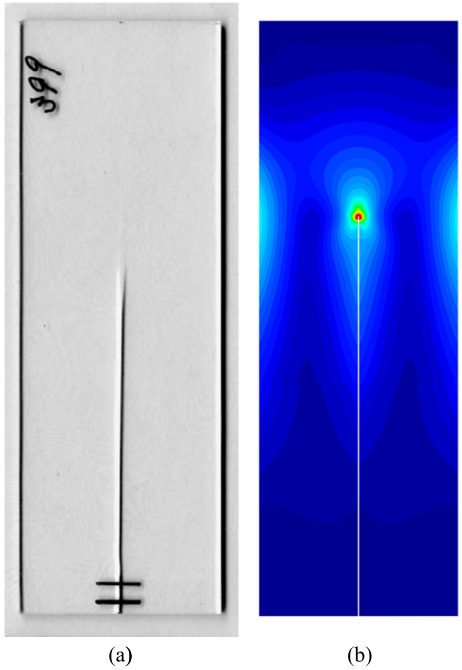

Fig. 10. The path of crack growth: (a) experimental result in [28], (b) present work.

is not enough time for heat transfer in the plate and the temperature gradients are small. But with the lapse of time and when the distance between hot and cold regions is reduced, the temperature gradients are intensified and this in turn will cause an increase in the displacement and in stress intensity factor K_I.

For a closer look at the stress contours and a quantitative comparison of them, a coordinate system (xy) is considered while its origin is attached to the crack tip, as it is shown in Fig. 12. A and B are the intersections of the x and y axis with the plate boundaries.

Fig. 13 shows the variations of the stress components along the vertical axis. The dash dot & dot lines, which are related to the present work, are in proximate agreement with the dash & solid lines, which belong to the experimental work [29].

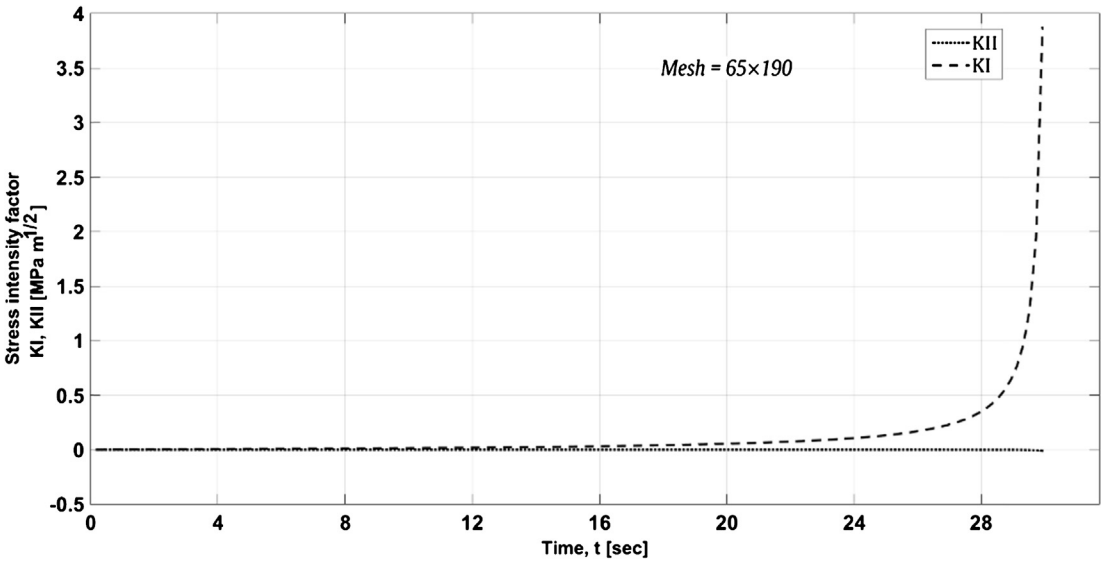

Fig. 11. Variations of the stress intensity factors over time.

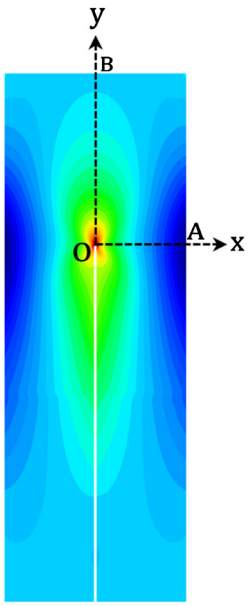

Fig. 12. The coordinate system defined for investigating the stress fields.

Fig. 14 and Fig. 15 show the variations of the stress fields along the axes of the specified coordinate system for the time when the plate had completely exited the furnace.

The results show that the XFEM formulation provides satisfactory numerical results for the above-mentioned problem, which is in good agreement with experimental results [28,29]. This formulation considered all affected parameters, so it can be appropriately used to study similar phenomena. This framework also can help factories to improve the production process through getting a better view and more exact data about the behavior of cracks in glass plates.

5. Conclusion

In the present study, the XFEM model for transient heat conduction in a moving glass plate is performed in order to investigate the stress field components and the Von Mises stress around the crack tip. In the XFEM formulation, convective heat exchange with moving boundaries was considered, in which the different convection coefficients and various temperatures of the various surrounding fluids were taken into account. Then, the Crank–Nicolson time integration scheme is developed and adjusted for accurately solving the global system of the ODE heat equations. Afterward, the contours of the

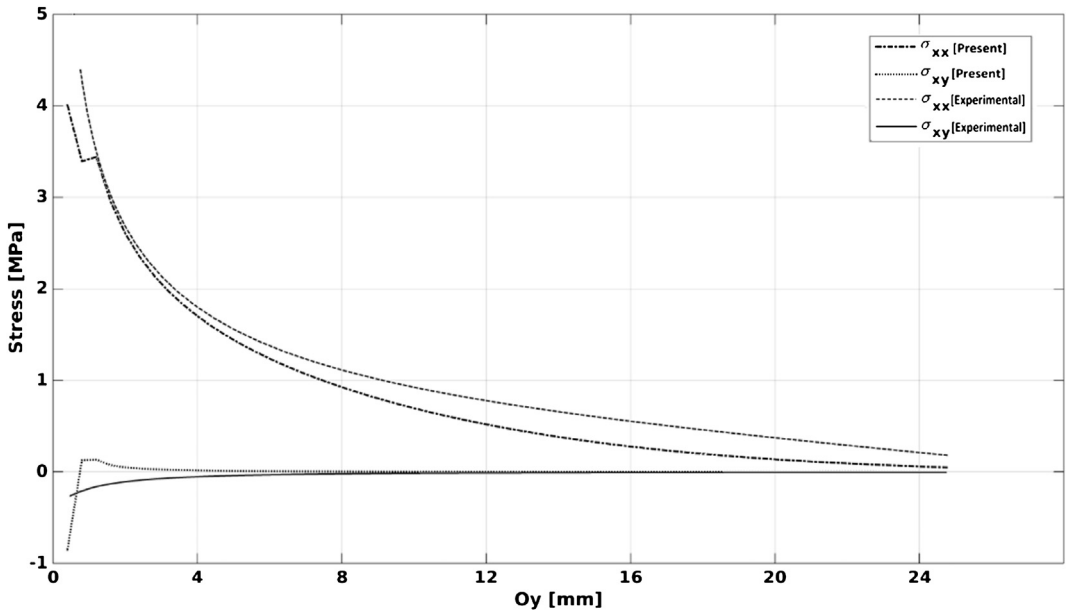

Fig. 13. Variations of stress fields along the vertical axis (Oy), (dash & solid lines: experimental curve in [29], dash dot & dot lines: present work).

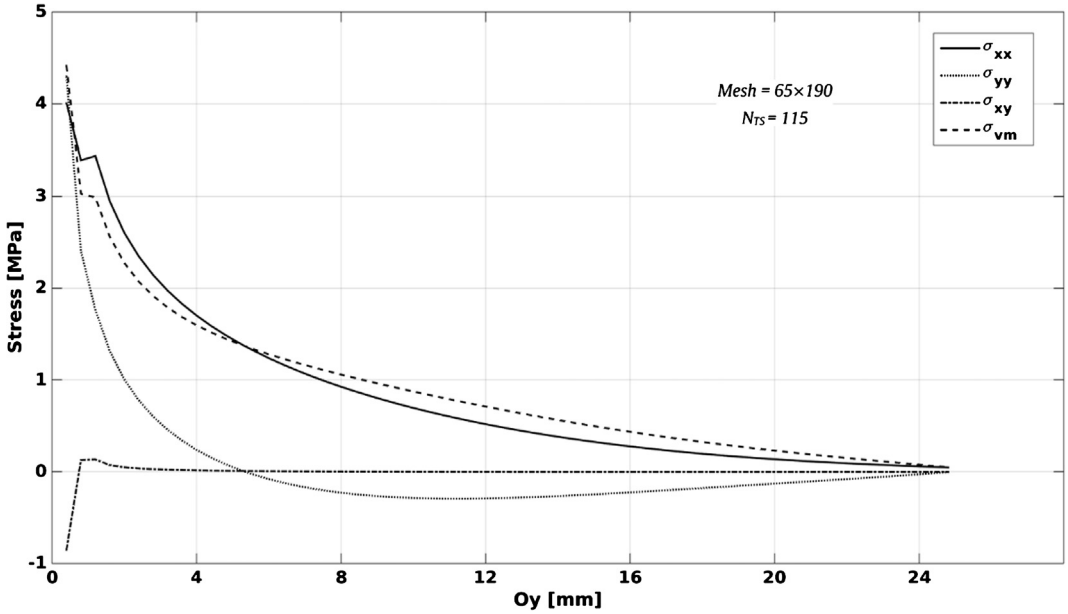

Fig. 14. Variations of stress fields along the vertical axis (Oy), for the time when the plate has completely exited the furnace.

stress field components as well as of the Von Mises stress were plotted. In order to display the ability of the developed formulation, the results were compared with experimental data from the literature. The results illustrated that a compressive stress region exists around the tensile stress area at the crack tip, which can be considered as a main cause for higher mode-I stress intensity factor, as it has been presented in the experimental results. The variations of the stress intensity factors versus time are depicted and, according to their magnitude, the K_I dominant state was considered to predict the crack propagation. The changes in the variations of the stresses created along the axes of a specified coordinate system attached to the crack tip are compared numerically. Generally, it can be stated that the XFEM presented here can help construct a better view of similar problems in order to improve the production process.

Appendix A

The defined terms of global stiffness, capacitance and conductance matrices are:

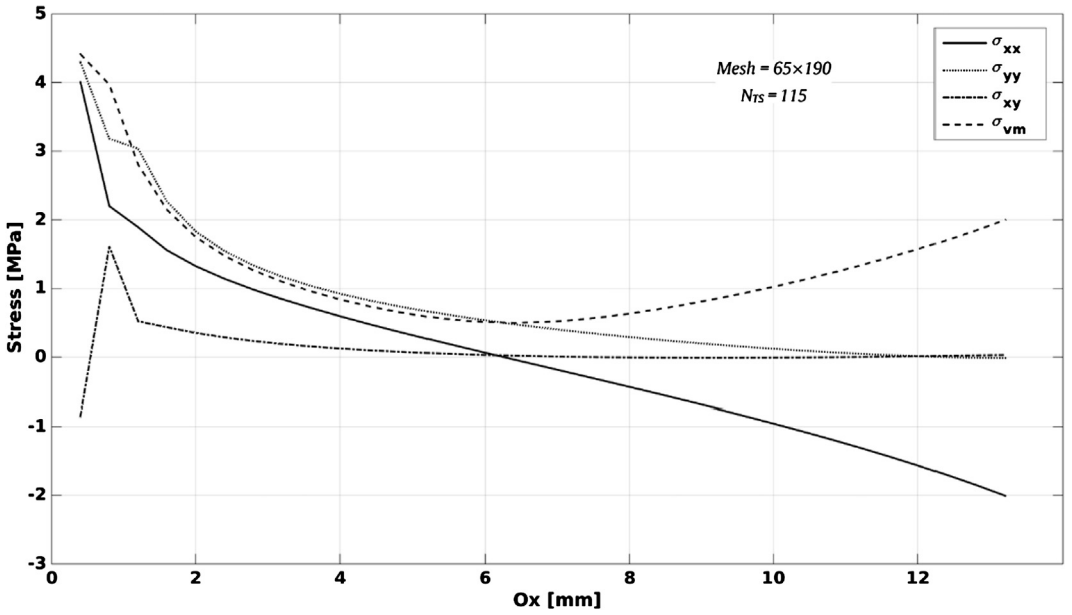

Fig. 15. Variations of stress fields along the horizontal axis (Ox) for the time when the plate has completely exited the furnace.

$$[B] = \begin{bmatrix} B_u & B_a & B_b \end{bmatrix} \qquad B_u = \begin{bmatrix} N_{,x} & 0 \\ 0 & N_{,y} \\ N_{,y} & N_{,x} \end{bmatrix} \qquad B_a = \begin{bmatrix} (NH)_{,x} & 0 \\ 0 & (NH)_{,y} \\ (NH)_{,y} & (NH)_{,x} \end{bmatrix} \qquad B_b = \begin{bmatrix} (NF)_{,x} & 0 \\ 0 & (NF)_{,y} \\ (NF)_{,y} & (NF)_{,x} \end{bmatrix}$$

$$\left[B^{\text{th}}\right] = \begin{bmatrix} B_T^{\text{th}} & B_A^{\text{th}} & B_B^{\text{th}} \end{bmatrix} \qquad B_T^{\text{th}} = \begin{bmatrix} N_{,x} \\ N_{,y} \end{bmatrix} \qquad B_A^{\text{th}} = \begin{bmatrix} (NH)_{,x} \\ (NH)_{,y} \end{bmatrix} \qquad B_B^{\text{th}} = \begin{bmatrix} (NF_1)_{,x} \\ (NF_1)_{,y} \end{bmatrix}$$

$$[\Psi] = \begin{bmatrix} N_T & N_A & N_B \end{bmatrix} \qquad N_T = [N] \qquad N_A = [NH] \qquad N_B = [NF_1]$$

$$[C] = \begin{bmatrix} \frac{E}{1-\nu^2} & \frac{\nu E}{1-\nu^2} & 0 \\ \frac{\nu E}{1-\nu^2} & \frac{E}{1-\nu^2} & 0 \\ 0 & 0 & \frac{E}{2(1+\nu)} \end{bmatrix} \qquad D = \begin{bmatrix} k & 0 \\ 0 & k \end{bmatrix}$$

The components of strain and stress fields as well as Von Mises stress are:

$$\{\varepsilon\} = \varepsilon_{ij} = \begin{Bmatrix} \varepsilon_{xx} \\ \varepsilon_{yy} \\ \varepsilon_{xy} \end{Bmatrix} = [B]\{U\}$$

$$\{\sigma\} = \sigma_{ij} = \begin{Bmatrix} \sigma_{xx} \\ \sigma_{yy} \\ \sigma_{xy} \end{Bmatrix} = [C]\{\varepsilon\}$$

$$\sigma_V = \sqrt{\sigma_{xx}^2 - \sigma_{xx}\sigma_{yy} + \sigma_{yy}^2 + 3\sigma_{xy}^2}$$

References

[1] T. Pin, T.H.H. Pian, On the convergence of the finite-element method for problems with singularity, Int. J. Solids Struct. 9 (1973) 313–321, http://dx.doi.org/10.1016/0020-7683(73)90082-6.
[2] T. Belytschko, T. Black, Elastic crack growth in finite elements with minimal remeshing, Int. J. Numer. Methods Eng. 45 (1999) 601–620.
[3] C.A. Duarte, J.T. Oden, Hp clouds—A meshless method to solve boundary-value problem, TICAM rep., 1995, pp. 5–95.
[4] J.M. Melenk, I. Babuška, The partition of unity finite-element method: basic theory and applications, Comput. Methods Appl. Mech. Eng. 139 (1996) 289–314.
[5] E. Goli, H. Bayesteh, S. Mohammadi, Mixed mode fracture analysis of adiabatic cracks in homogeneous and non-homogeneous materials in the framework of partition of unity and the path-independent interaction integral, Eng. Fract. Mech. 131 (2014) 100–127.
[6] A. Yazid, N. Abdelkader, H. Abdelmadjid, A state-of-the-art review of the X-FEM for computational fracture mechanics, Appl. Math. Model. 33 (2009) 4269–4282.
[7] A. Zamani, M.R. Eslami, Implementation of the extended finite-element method for dynamic thermoelastic fracture initiation, Int. J. Solids Struct. 47 (2010) 1392–1404.
[8] M. Duflot, The extended finite-element method in thermoelastic fracture mechanics, Int. J. Numer. Methods Eng. 74 (2008) 827–847.

[9] K.Y. Lam, T.E. Tay, W.G. Yuan, Stress intensity factors of cracks in finite plates subjected to thermal loads, Eng. Fract. Mech. 43 (1992) 641–650.
[10] M.R. Ayatollahi, M.R.M. Aliha, Mixed mode fracture in soda lime glass analyzed by using the generalized MTS criterion, Int. J. Solids Struct. 46 (2009) 311–321.
[11] Y. Hayakawa, Numerical study of oscillatory crack propagation through a two-dimensional crystal, Phys. Rev. E 49 (1994) R1804.
[12] M. Marder, Instability of a crack in a heated strip, Phys. Rev. E 49 (1994) R51.
[13] S. Sasa, K. Sekimoto, H. Nakanishi, Oscillatory instability of crack propagations in quasistatic fracture, Phys. Rev. E 50 (1994) R1733.
[14] H.-A. Bahr, A. Gerbatsch, U. Bahr, H.-J. Weiss, Oscillatory instability in thermal cracking: a first-order phase-transition phenomenon, Phys. Rev. E 52 (1995) 240.
[15] M. Adda-Bedia, Y. Pomeau, Crack instabilities of a heated glass strip, Phys. Rev. E 52 (1995) 4105–4113, http://dx.doi.org/10.1103/PhysRevE.52.4105.
[16] B.D. Ferney, M.R. DeVary, K.J. Hsia, A. Needleman, Oscillatory crack growth in glass, Scr. Mater. 41 (1999) 275–281.
[17] Y. Pomeau, Fundamental problems in brittle fracture: unstable cracks and delayed breaking, C. R. Mecanique 330 (2002) 249–257, http://dx.doi.org/10.1016/S1631-0721(02)01456-0.
[18] E. Bouchbinder, H.G.E. Hentschel, I. Procaccia, Dynamical instabilities of quasistatic crack propagation under thermal stress, Phys. Rev. E 68 (2003) 36601.
[19] K. Sakaue, R. Yamada, M. Takashi, A study on propagation patterns of thermally induced cracks in a brittle solid, Nippon Kikai Gakkai Ronbunshu A Hen (Trans. Jpn. Soc. Mech. Eng. Part A) (Japan) 18 (2006) 1697–1702.
[20] K. Sakaue, M. Takashi, Experimental investigation of crack path instabilities in a quenched plate, in: Proc. 2006 SEM Annu. Conf. Expo. Exp. Appl. Mech. Soc. Exp. Mech. Bethel, Pap., 2006.
[21] A. Yuse, M. Sano, Transition between crack patterns in quenched glass plates, Nature 362 (1993) 329–331.
[22] O. Ronsin, B. Perrin, Dynamics of quasistatic directional crack growth, Phys. Rev. E 58 (1998) 7878.
[23] B. Yang, K. Ravi-Chandar, Crack path instabilities in a quenched glass plate, J. Mech. Phys. Solids 49 (2001) 91–130.
[24] S. Yoneyama, H. Kikuta, K. Moriwaki, Simultaneous observation of phase-stepped photoelastic fringes using a pixelated microretarder array, Opt. Eng. 45 (2006) 83604.
[25] S. Yoneyama, K. Sakaue, H. Kikuta, M. Takashi, Instantaneous phase-stepping photoelasticity for the study of crack growth behaviour in a quenched thin glass plate, Meas. Sci. Technol. 17 (2006) 3309.
[26] K. Sakaue, S. Yoneyama, H. Kikuta, M. Takashi, Evaluating crack tip stress field in a thin glass plate under thermal load, Eng. Fract. Mech. 75 (2008) 1015–1026.
[27] S. Yoneyama, K. Sakaue, H. Kikuta, M. Takashi, Observation of stress field around an oscillating crack tip in a quenched thin glass plate, Exp. Mech. 48 (2008) 367–374.
[28] K. Sakaue, S. Yoneyama, M. Takashi, Study on crack propagation behavior in a quenched glass plate, Eng. Fract. Mech. 76 (2009) 2011–2024.
[29] S. Yoneyama, K. Sakaue, Experimental–numerical hybrid stress analysis for a curving crack in a thin glass plate under thermal load, Eng. Fract. Mech. 131 (2014) 514–524.
[30] I. Babuška, J.M. Melenk, The partition of unity method, Int. J. Numer. Methods Eng. 40 (1997) 727–758, http://dx.doi.org/10.1002/(SICI)1097-0207(19970228)40:4<727::AID-NME86>3.0.CO;2-N.
[31] M. Pais, N.-H. Kim, T. Davis, Reanalysis of the extended finite-element method for crack initiation and propagation, in: Proc. AIAA Struct. Struct. Dyn. Mater. Conf., 2010.
[32] N. Moës, J. Dolbow, T. Belytschko, A finite-element method for crack growth without remeshing, Int. J. Numer. Methods Eng. 46 (1999) 131–150.
[33] S. Osher, J.A. Sethian, Fronts propagating with curvature-dependent speed: algorithms based on Hamilton–Jacobi formulations, J. Comput. Phys. 79 (1988) 12–49.
[34] S. Osher, R.P. Fedkiw, Level set methods: an overview and some recent results, J. Comput. Phys. 169 (2001) 463–502.
[35] M. Stolarska, D.L. Chopp, N. Moës, T. Belytschko, Modelling crack growth by level sets in the extended finite-element method, Int. J. Numer. Methods Eng. 51 (2001) 943–960, http://dx.doi.org/10.1002/nme.201.
[36] T. Belytschko, N. Moës, S. Usui, C. Parimi, Arbitrary discontinuities in finite elements, Int. J. Numer. Methods Eng. 50 (2001) 993–1013.
[37] M. Fleming, Y.A. Chu, B. Moran, T. Belytschko, Y.Y. Lu, L. Gu, Enriched element-free Galerkin methods for crack tip fields, Int. J. Numer. Methods Eng. 40 (1997) 1483–1504.
[38] A.F. Bower, Applied Mechanics of Solids, CRC Press, 2009.
[39] A. Ahmed, F. Auricchio, Extended finite-element method (XFEM)-modeling arbitrary discontinuities and failure analysis, Res. degree thesis, 2009.
[40] R.J. Astley, Finite Elements in Solids and Structures. An Introduction, Chapman & Hall (Springer), 1992.
[41] H.M. Westergaard, Bearing pressures and cracks, J. Appl. Mech. 61 (1939) A49–A53.
[42] M.L. Williams, On the stress distribution at the base of a stationary crack, J. Appl. Mech. 24 (1957) 109–114, http://dx.doi.org/10.1115/1.3640470.
[43] M. Pais, Matlab extended finite element (MXFEM) code v1.2, www.matthewpais.com, 2011.
[44] M.N. Ozisik, Heat Conduction, John Wiley & Sons, 1993.
[45] D.V. Hutton, J. Wu, Fundamentals of Finite Element Analysis, McGraw-Hill, New York, 2004.
[46] R.B. Hetnarski, Encyclopedia of Thermal Stresses, Springer, 2014.
[47] S. Moaveni, Finite Element Analysis: Theory and Application with ANSYS, Pearson Education, India, 2003.
[48] J.G. Charney, R. Fjörtoft, J. Von Neumann, Numerical integration of the barotropic vorticity equation, Tellus 2 (4) (1950) 237–254.